NANOMATERIALS
SCIENCE & ENGINEERING
Vol. 2, No. 4, pp. 162-169 (2020)

RESEARCH ARTICLE

https://doi.org/10.34624/nmse.v2i4.21063

Photocatalytic degradation of organic pollutant using TiO_2/rGO nanocomposites under simulated sunlight

Martina Kocijan[1, *], **Lidija Ćurković**[1], **Tina Radošević**[2], **Matejka Podlogar**[2]

[1] Department of Materials, Faculty of Mechanical Engineering and Naval Architectur University of Zagreb, Ivana Lučića 5, 10000 Zagreb, Croatia
[2] Department for Nanostructured Materials, Jožef Stefan Institute, Jamova cesta 39, SI-1000, Ljubljana, Slovenia
**Corresponding author, e-mail address: martina.kocijan@fsb.hr*

Received 6 June 2020; accepted 1 December 2020; published online 15 December 2020

ABSTRACT

Here, we present the development and performance of a nanocomposite photocatalyst based on titanium dioxide (TiO_2) and reduced graphene oxide (rGO). The material was prepared using a direct sol-gel method, followed by hydrothermal treatment. Different experimental conditions, such as time and temperature during the synthesis, were investigated with the aim to optimize photocatalytic degradation. The influence of the preparation conditions on the physicochemical properties of the synthesized powders was established by different characterization methods such as Scanning Electron Microscopy (SEM), and Raman spectroscopy. The effectiveness of the synthesized photocatalysts was examined through the photodegradation of caffeine under simulated sunlight irradiation. The influence of synthesized parameters on the TiO_2/rGO performance for the photodegradation of pharmaceutical caffeine was monitored by UV-Vis spectroscopy.

The obtained results show that the photocatalytic properties of the prepared TiO_2/rGO composites depend on different experimental parameters of their synthesis procedure, such as time and temperature. The TiO_2/rGO_6/400 composite presents a very efficient photo-degradation of caffeine by simulated sunlight irradiation, resulting in an efficiency of 95% within 90 minutes.

1. INTRODUCTION

At the beginning of the 21st century, mankind has to face the problem of unavailability of water as an important threat, due to the loss of the balance between the quantity and quality of this important resource. The ubiquitous pollutants such as drugs, pesticides, personal care products, and organic dyes, also known as emerging organic pollutants (EOP) have become a matter of increasing concern. They have raised considerable worries due to their frequent occurrence in drinking water, groundwater, and surface water, although in very low concentrations [1,2].

High concentrations of Caffeine ($C_8H_{10}N_4O_2$, CAF) can be found in natural sorts, such as cacao seeds and coffee beans, and also in processed products (e.g. coffee, energy drinks, chocolates, and tea) [3–5]. The pharmaceutical industry is using CAF as an elementary compound for producing a variety of drugs that are used in medical therapy. Caffeine is the most frequently detected pharmaceutical in the groundwaters, and surface waters worldwide. The CAF in aqueous solutions, which has a high-water solubility of more than 10.0 mg/L, has negative effects on the environment. It is toxic for living organisms and it has a high resistance to natural degradation [3,4].

Advanced oxidation processes represent a facile route to remove EOP from the water and wastewater environment. Among them, photocatalysis [6,7], photo-Fenton [8], and ozonation [9] appears the most appealing. Within this study, we investigated factors affecting the photocatalytic degradation of caffeine under simulated sunlight irradiation.

This study reports the photocatalytic degradation of CAF using TiO_2/rGO composites. Apart from the synthesis factors (time and temperature) affecting the photocatalytic degradation, an important aspect of this research was to understand how to synthesize the GO and TiO_2/rGO composites.

2. METHODS

2.1. Chemicals and Reagents

Commercially available natural graphite flakes (particle size ≤ 50 μm) and titanium (IV) isopropoxide ($Ti(C_3H_5O_{12})_4$, TTIP, 97%) were purchased from Sigma-Aldrich. Concentrated sulfuric acid (H_2SO_4, 95%-97%), and concentrated nitric acid (HNO_3, ≥65%) were obtained from Fluka and Lab Expert, respectively. Concentrated hydrochloric acid (HCl, 37%), potassium permanganate ($KMnO_4$), sodium nitrate ($NaNO_3$), hydrogen peroxide (H_2O_2, 30% w/v), *i*-propanol (C_3H_7OH), acetylacetone ($CH_3(CO)CH_2(CO)CH_3$) were supplied from Gram mol. The solutions with stated chemicals were prepared using ultrapure water (Millipore) obtained with a Direct-Q Millipore system.

2.2. Synthesis of graphene oxide (GO)

GO was synthesized by Hummer's method [10]. Firstly, flake-like graphite powder (3 g) was dispersed in H_2SO_4 (69 mL) and $NaNO_3$ (1.5 g) by magnetic stirring (30 min) at low temperature (0-5 °C). Then $KMnO_4$ (9.0 g) was dropwise added, to keep the reaction temperature lower than 20 °C. After addition, the mixture was heated to 35 °C and stirred for 30 min at which time water (138 mL) was slowly added. The process initiated an exothermic reaction, which gave rise to spontaneous heating to 98 °C. Additional heating was subsequently introduced to maintain the temperature at 98 °C for an additional 15 min, after which the reaction vessel was cooled down in a water bath. Additional water (420 mL) and 30% H_2O_2 (3 mL) were added one more time, resulting in another exothermic reaction. After the reaction mixture was cooled to room temperature, the resultant suspension was centrifugated at 3000 rpm for 10 minutes to remove remaining impurities and to isolate the graphite oxide (GO). GO was first washed with dilute HCl (10%) and then with deionized water several times to produce a slurry of GO with a neutral pH.

2.3. Preparation of TiO_2 sol (colloidal solution)

TiO_2 sol was prepared using titanium (IV) isopropoxide (TTIP) as a precursor, *i*-propanol (PrOH) as a solvent, acetylacetone (AcAc) as a chelating agent and nitric acid (HNO_3) as a catalyst. The molar ratio of the reactants was: TTIP:PrOH:AcAc:HN = 1:35:0.63:0.015 [11].

2.4. Preparation of TiO_2/rGO nanocomposites

TiO_2/rGO composites were synthesized by the *in situ* procedure, using the TiO_2 colloidal sol prepared by the sol-gel route, which was hydrothermally treated in the presence of the GO substrates. The prepared slurry of GO was added into a colloidal solution of TiO_2 sol and stirred for 1 h until the liquid became a black-brown suspension. After that, the liquid was homogenized for 10 min in an ultrasonic bath. Subsequently, the suspension was transferred into a Teflon-lined autoclave and kept at 180 ℃ during the next 4 and 6 hours. The containers were removed from the oven and cooled to ambient temperature. The synthesized nanocomposite was washed to neutral pH value with *i*-propanol and deionized water and dried in an oven at 60 ℃ for 1 h. Finally, the synthesized powders were calcinated at 300 ℃ and 400 ℃ respectively. The obtained composites contained 5 wt.% of rGO and they were labelled TiO_2/rGO_4/300,TiO_2/rGO_6/400,TiO_2/rGO_4/300 and TiO_2/rGO_6/400.

2.5. Characterization of photocatalyst

The microstructural characteristics of the samples were obtained using scanning electron microscopy (SEM). Measurements were made with Jeol JEM-2100 equipment. The crystalline phases of the synthesized composites were analyzed by Raman microscope (NT-MDT Spectra II) using the Raman excitation energy at 633 nm.

2.6. Photocatalytic activity

To test the photocatalytic activity of the prepared nanocomposites, 9 mg of the synthesized photocatalyst were dispersed in the 9 mL of caffeine solution (10 mg/mL) and irradiated with simulated solar light (lamp: ULTRA-VITALUX, 230 V, 300 W, Osram) for 90 minutes. The degradation process was monitored by UV-Vis spectroscopy, taking aliquots at regular intervals (every 30 min). Each aliquot was centrifuged to remove the catalyst and, the resulting clear liquid was analyzed. The absorbance was recorded by a UV-Vis spectrophotometer (Lambda 950 Spectrophotometer, PerkinElmer) in the range from 200 to 400 nm using quartz cells with a path length of 10 mm.

Before the photocatalytic test, the prepared suspensions were kept in the dark for 30 minutes to achieve the adsorption equilibrium. The adsorption process in the dark was also monitored by UV-Vis spectroscopy.

3. RESULTS AND DISCUSSION

3.1. Characterization of photocatalyst

The representative morphologies of the synthesized GO and composites were evaluated by Scanning Electron Microscopy (SEM), as depicted in Fig.1. Fig.1A shows the SEM image of GO layers, indicating that GO is full of wrinkles and consists of thin layers. The size and the number of layers is similar to reported investigations [12,13]. The morphology of the composite photocatalyst is significantly different compared to pure GO. Fig. 1B represents the TiO_2-rGO_6/300 composite. Small uneven agglomerates of TiO_2 particles can be found growing out from the GO surface [13].

The Raman spectra of synthesized materials are shown in Fig. 3. For both TiO_2-rGO composites, the characteristic peaks of the anatase phase are present. These peaks are at 158.5 cm^{-1}, 404.3 cm^{-1}, 519.5 cm^{-1}, and 638.7 cm^{-1} for the sample TiO_2-rGO_6/300, and 157.3 cm^{-1}, 401.9 cm^{-1}, 521.7 cm^{-1}, and 644 cm^{-1} for the sample TiO_2/rGO_6/400. Individual peaks are attributed to Eg, B1g, A1g+B1g, and Eg Raman modes. The rutile phase is not present in the synthesized composites [14]. Furthermore, it can be clearly seen that the Raman spectra of synthesized composites show characteristic peaks of graphene materials, which correspond to the D and G band (Table 1). The vibrations of the D and G peaks in rGO materials were significantly shifted compared to pure GO material. The laser excitation energy is the reason for the changes in peaks position in materials [13]. In our investigation, a laser with a wavelength of 633 nm was used. The reason for shifting is also in the changes of the graphene structure. Explicitly the G band represents the sp^2 hybridization in C-C bonds and the intensity of the D band corresponds to the sp^3 hybridization which is in this structure associated with structural defects on the boundary [15]. Since the absolute intensity is difficult to determine from a solid-state sample

Figure 1. Synthetized graphene oxide slurry by Hummer's method.

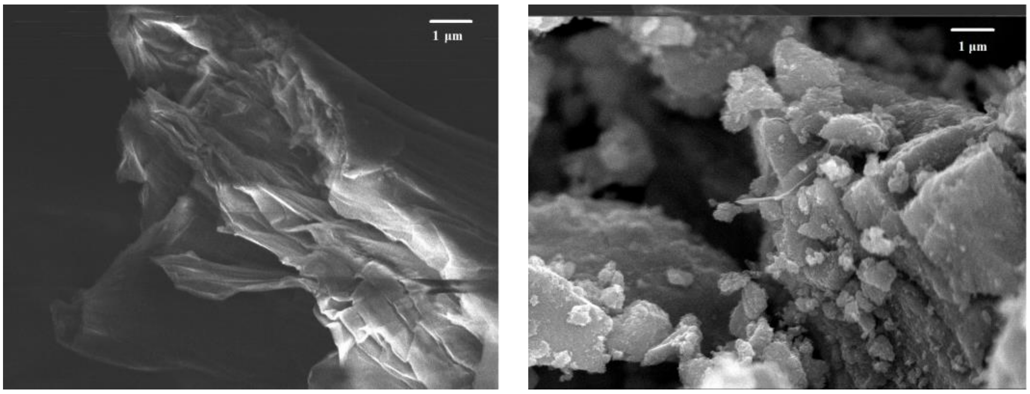

Figure 2. SEM images of synthesized GO (left image), and TiO_2-rGO_6/300 composite (right image).

the intensity ratios between D and G peaks are more informative. It shows that the number of defects grows gradually from graphene where it is expectedly the smallest, to the composite with TiO_2, where the ratio is the highest, as shown in Fig. 3 and Table 1.

The ratio of intensities between D and G bands is utilized to determine the crystal size parallel to basal planes (*La*), using the equation of Tuinstra

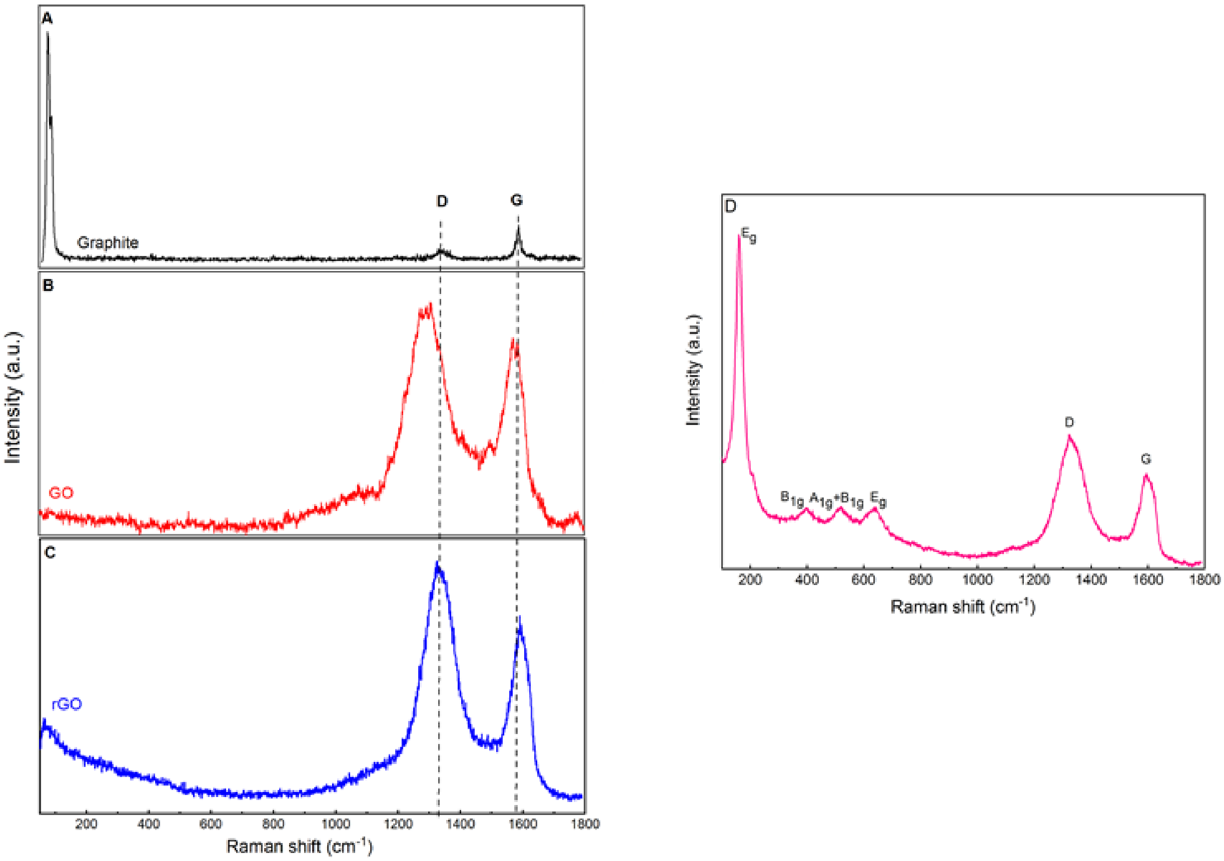

Figure 3. Raman spectra of (A) graphite, (B) graphene oxide (GO), (C) reduced graphene oxide (rGO), and (D) the respective TiO_2/rGO nanocomposite.

Table 1. Raman intensity and shift for the prepared materials.

Samples	***D*-band, cm^{-1}**	**I_D**	***G*-band, cm^{-1}**	**I_G**	**I_D/I_G**	**L_a, nm**
Graphite	1327.8	405	1583.5	579	0.70	55
GO	1348.0	139	1605.0	123	1.13	34
rGO	1325.8	774	1590.5	631	1.22	31
TiO_2/rGO_6/300	1331.0	327	1595.5	235	1.39	27

and Koenig, where the coefficient 38.5 is for measurements at 633 nm [16]:

$$L_a(nm) = \frac{38.5}{I_D/I_G} \quad (1)$$

The L_a values are 55 nm for graphite, 34 nm for GO, 31 nm for rGO, and 27 nm for TiO_2/rGO as shown in Table 1. A lower L_a value demonstrates a decrease of sp^2 domains in the prepared materials.

3.2. Photocatalytic activity

The change in the maximum absorption peak for caffeine versus the irradiation time under simulated sunlight is shown in Fig. 4A-D. The maximum of the

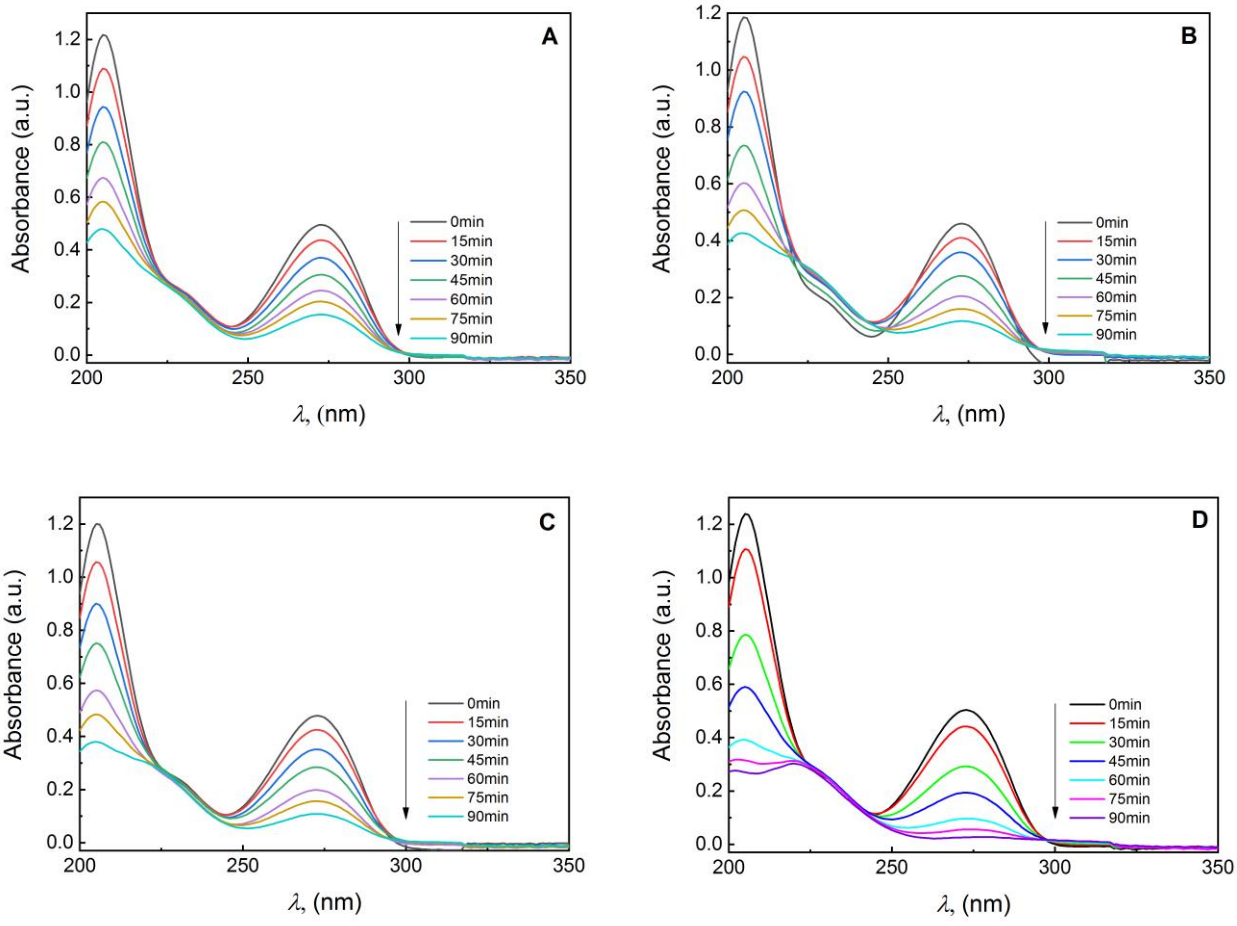

Figure 4. The absorption spectra for photo-degradation of caffeine as a function of irradiation interval in the presence of catalysts (A) TiO_2/rGO_4/300, (B) TiO_2/rGO_4/400, (C) TiO_2/rGO_6/300, and (D) TiO_2/rGO_6/400.

peak at 274 nm decreases with the longer irradiation time. The same trend can be observed for all four measured photocatalysts.

The performance of different TiO_2/rGO composites was evaluated based on the degradation of caffeine, shown in Fig. 5A. The degradation of caffeine was monitored through the change of its characteristic peak at 274 nm. Firstly, the adsorption in the dark was monitored for 30 minutes and subsequently, photocatalytic degradation of caffeine under simulated sunlight irradiation was measured, up to 90 minutes. Upon reaching the adsorption-desorption equilibrium (30 minutes), the irradiation source was turned on and the concentration of caffeine in the observed suspensions started to decrease, as seen in Fig. 5A. Results indicate that the caffeine was photo-degraded using the prepared TiO_2/rGO composites, as displayed in Fig. 5B.

The percentage of photoactivity of the synthesized photocatalysts, shown in Fig. 5C was calculated using the equation:

$$\eta = \frac{A_0 - A_t}{A_0} * 100\% \qquad (2)$$

where, η is the percentage of the caffeine degradation, A_0 is the absorbance of the initial caffeine concentration (before irradiation) and A_t is the concentration of caffeine at time *t*, expressed as absorbance after irradiation at the determined time, *t* (min), during the whole photocatalytic process.

The first-order rate constant is calculated by the slope of the straight line obtained from plotting linear regression of $-ln(A/A_0)$ versus irradiation time, *t,* as shown in Fig. 5D, and represented with the following equation [17]:

$$A_t = A_0 * e^{-k*t} \qquad (3)$$

where, *k* (min^{-1}) is the degradation rate constant, A_t is the absorption of caffeine at the time of the photocatalytic process and A_0 is the absorption at the beginning of the experiment.

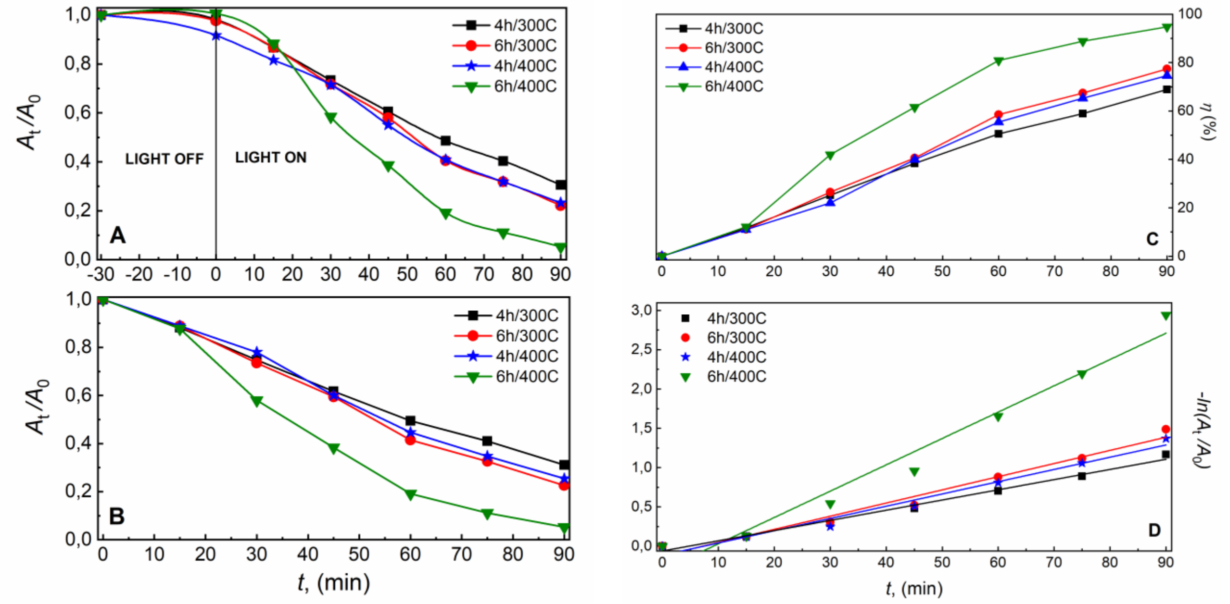

Figure 5. (A) Time evolution of CAF concentration in the presence of the as-prepared catalysts in the dark and under simulated sunlight irradiation, (B) time evolution of relative CAF concentration using synthesized composites, (C) photocatalytic degradation of CAF in percentage at different time, (D) first-order kinetic curves of the CAF degradation.

Table 2. Photo-degradation kinetics of caffeine under simulated sunlight irradiation.

Sample	R^2	$k\times10^{-3}$, min^{-1}	$t_{1/2}$, min
TiO_2/rGO_4/300	0.9942	4.56	152.00
TiO_2/rGO_6/300	0.9880	7.12	97.35
TiO_2/rGO_4/400	0.9894	6.22	111.44
TiO_2/rGO_6/400	0.9882	19.5	35.55

The half-life ($t_{1/2}$) was calculated by the following equation [18]:

$$t_{1/2} = \frac{\ln(2)}{k} \quad (4)$$

Caffeine degradation efficiency increases from 69%, 75%, 77% to 95% for TiO_2/rGO_4/300, TiO_2/rGO_4/400, TiO_2/rGO_6/300, and TiO_2/rGO_6/400, respectively, after 90 min under simulated sunlight irradiation, Fig. 5C

In Table 2 the coefficient of determination (R^2), the reaction rate constant ($k\times10^{-3}$), and half-life photo-degradation rate ($t_{1/2}$) are collected. The reaction rate constant and half-life of degradation were calculated for the composites, assuming the photo-degradation process followed the first-order kinetics model. The coefficient of determination is very high, proving first-order kinetics for the photocatalytic degradations. The reaction rate constant and the half-life degradation rate of TiO_2/rGO_4/300, TiO_2/rGO_4/400, and TiO_2/rGO_6/300 photocatalysts show slower removal of caffeine than TiO_2/rGO_6/400 photocatalyst, as depicted in Fig. 5A., the following was confirmed with constants in Table 2.

4. CONCLUSION

The GO was successfully prepared by Hummer's method. The TiO_2/rGO composites were effectively synthesized by exploring the two-step method that combines simple hydrothermal and calcination treatment. The successful synthesis of the composite was closely associated with the time of hydrothermal synthesis, and calcination temperature. Photocatalytic properties of powders were determined by the degradation of caffeine under simulated sunlight irradiation.

These results show that the composites successfully synthesized with the proposed method can be used for the decomposition of caffeine by simulated sunlight. The TiO_2/rGO composites can also be used as highly efficient and "green" photocatalysts in effluent water treatment if the surface is exposed to sunlight.

REFERENCES

[1] G. Luna-Sanguino, A. Tolosana-Moranchel, C. Duran-Valle, M. Faraldos, A. Bahamonde, Optimizing P25-rGO composites for pesticides degradation: Elucidation of photo-mechanism, *Catal. Today.* **328**, 172–177 (2019).

[2] X. Sun, S. Ji, M. Wang, J. Dou, Z. Yang, H. Qiu, S. Kou, Y. Ji, H. Wang, Fabrication of porous TiO_2-RGO hybrid aerogel for high-efficiency, visible-light photodegradation of dyes, *J. Alloys Compd.* **819**, 153033 (2020).

[3] M. Ghosh, K. Manoli, X. Shen, J. Wang, A.K. Ray, Solar photocatalytic degradation of caffeine with titanium dioxide and zinc oxide nanoparticles, *J. Photochem. Photobiol. A Chem.* **377**, 1–7 (2019).

[4] A. Elhalil, R. Elmoubarki, M. Farnane, A. Machrouhi, M. Sadiq, F.Z. Mahjoubi, S. Qourzal, N. Barka, Photocatalytic degradation of caffeine as a model pharmaceutical pollutant on Mg doped ZnO-Al_2O_3 heterostructure, *Environ. Nanotechnology, Monit. Manag.* **10**, 63–72 (2018).

[5] A.J.S.C. Vieira, E.M. Gaspar, P.M.P. Santos, Mechanisms of potential antioxidant activity of caffeine, *Radiat. Phys. Chem.* **174**, 108968 (2020).

[6] R.R.N. Marques, M.J. Sampaio, P.M. Carrapiço, C.G. Silva, S. Morales-Torres, G. Dražić, J.L. Faria, A.M.T. Silva, Photocatalytic degradation of caffeine: Developing solutions for emerging pollutants, *Catal. Today.* **209**, 108–115 (2013).

[7] M.K. Arfanis, P. Adamou, N.G. Moustakas, T.M. Triantis, A.G. Kontos, P. Falaras, *Chem. Eng. J.* **310**, 525-536 (2017).

[8] A.G. Trovó, T.F.S. Silva, O. Gomes, A.E.H. Machado, W.B. Neto, P.S. Muller, D. Daniel, Degradation of caffeine by photo-Fenton process: Optimization of treatment conditions using experimental design, *Chemosphere.* **90**,170–175 (2013).

[9] R. Rosal, A. Rodríguez, J.A. Perdigón-Melón, A. Petre, E. García-Calvo, M.J. Gómez, A. Agüera, A.R. Fernández-Alba, Degradation of caffeine and identification of the transformation products generated by ozonation, *Chemosphere.* **74**, 825–831 (2009).

[10] D.C. Marcano, D. V. Kosynkin, J.M. Berlin, A. Sinitskii, Z. Sun, A. Slesarev, L.B. Alemany, W. Lu, J.M. Tour, Improved synthesis of graphene oxide, *ACS Nano.* **4**, 4806–4814 (2010).

[11] M. Čizmić, D. Ljubas, L. Ćurković, I. Škorić, S. Babić, Kinetics and degradation pathways of photolytic and photocatalytic oxidation of the anthelmintic drug praziquantel, *J. Hazard. Mater.* **323** 500–512 (2017).

[12] S. Gurunathan, J.W. Han, V. Eppakayala, J.H. Kim, Green synthesis of graphene and its cytotoxic effects in human breast cancer cells, *Int. J. Nanomedicine.* **8**, 1015–1027 (2013).

[13] E. Kusiak-Nejman, A. Wanag, J. Kapica- Kozar, Ł. Kowalczyk, M. Zgrzebnicki, B. Tryba, J. Przepiórski, A.W. Morawski, Methylene blue decomposition on TiO_2/reduced graphene oxide hybrid photocatalysts obtained by a two-step hydrothermal and calcination synthesis, *Catal. Today.* **357**, 630-637 (2019).

[14] M. Mohammadi, M. Rezaee Roknabadi, M. Behdani, A. Kompany, Enhancement of visible and UV light photocatalytic activity of rGO-TiO_2 nanocomposites: The effect of TiO_2/Graphene oxide weight ratio, *Ceram. Int.* **45**, 12625–12634 (2019).

[15] P. Wang, J. Wang, X. Wang, H. Yu, J. Yu, M. Lei, Y. Wang, One-step synthesis of easy-recycling TiO_2-rGO nanocomposite photocatalysts with enhanced photocatalytic activity, *Appl. Catal. B Environ.* **132–133**, 452–459 (2013).

[16] M. Pawlyta, J.N. Rouzaud, S. Duber, Raman microspectroscopy characterization of carbon blacks: Spectral analysis and structural information, *Carbon* **84**, 479–490 (2015).

[17] Y. Yang, L. Xu, H. Wang, W. Wang, L. Zhang, TiO_2/graphene porous composite and its photocatalytic degradation of methylene blue, *Mater. Des.* **108**, 632–639 (2016).

[18] X. Zhou, S. Zhou, F. Ma, Y. Xu, Synergistic effects and kinetics of rGO-modified TiO_2 nanocomposite on adsorption and photocatalytic degradation of humic acid, *J. Environ. Manage.* **235**, 293–302 (2019).